Proceedings of the 9th International Conference on Aluminium Alloys (2004)
Edited by J.F. Nie, A.J. Morton and B.C. Muddle

Control of Microstructure in a Spraycast Al-Mg-Li-Zr Alloy

S.C. Hogg, I.G. Palmer, P.S. Grant

Department of Materials, Parks Road, Oxford, OX1 3PH, U.K.

Keywords: Al-Mg-Li-Zr, spraycasting, EBSD, Zener-Holloman

Abstract

This paper describes the microstructural investigation of an Al-5.31Mg-1.15Li-0.28Zr alloy produced by spraycasting. Following a dispersoid precipitation treatment of 4h at 400°C, cylindrical samples were hot compressed to a range of total strains and a range of strain rates at temperatures between 250-400°C. Electron backscattered diffraction showed a strong dependence of grain size on compression temperature with new grains nucleating at regions of microscopic strain localisation such as triple points and grain boundaries. There was an inverse relationship between the size of these new grains and the Zener-Holloman factor during compression. The microstructures from the small scale compression experiments have been compared with those of larger scale forgings, and indicated that under similar conditions, microstructural evolution was broadly similar.

1. Introduction

Al-Mg-Li alloys offer the potential to reduce weight and improve performance in structural aerospace applications and alloys developed using conventional casting routes have provided excellent properties [1]. Critical to the alloy performance is the use of sometimes complex heat treatments that may result in quench cracking/distortion. Non-heat-treatable mechanically alloyed (MA) materials offering similar or enhanced properties have also been developed [2], but only in small quantities. The sub-micron grain sizes typical of MA materials may also have deleterious effects on the alloy fatigue crack growth rates because of reduced crack closure effects, and thermal stability during hot working. Spraycast Al-Mg-Li alloys offer the potential for microstructural refinement, extended alloying capability and reduced levels of embrittling elements associated with Li (Na, K and H) [3]. As part of a wider study to develop a spraycast non-heat-treatable Al-Mg-Li alloy of intermediate 1-5µm grain size, this paper presents an investigation of the microstructure of a spraycast Al-Mg-Li-Zr alloy and its microstructural evolution during post-spray hot compression as a function of temperature, strain, and strain rate.

2. Experimental

An Al-Mg-Li-Zr alloy with the composition given in Table 1 was spraycast at Oxford University, using conditions described elsewhere [4].

Table 1: Chemical composition of the Al-Mg-Li-Zr alloy (in weight percent, unless otherwise stated).

Mg	Li	Zr	Fe	Si	Na	K	Ca
5.31	1.15	0.28	0.03	0.02	6 ppm	<5 ppm	14 ppm

Material taken from the central region of the 26kg billet was hot consolidated at 100MPa at 400°C for 2 h in a closed die to remove any as-sprayed porosity, followed by a further 2h at 400°C in a resistance furnace and quenching to complete the dispersoid precipitation treatment. 8mmØ x 10mm samples of the consolidated material were then hot compressed under the range of conditions given in Table 2.

Table 2: Temperature, strain and strain rate used for hot compression experiments.

Designation	400-1-2	400-1-3	400-1.7-2	400-1.7-3	325-1-3	250-1-2	250-1-3	250-1.7-3
Temperature (°C)	400	400	400	400	325	250	250	250
True Strain	1	1	1.7	1.7	1	1	1	1.7
Strain rate (s^{-1})	$1x10^{-2}$	$1x10^{-3}$	$1x10^{-2}$	$1x10^{-3}$	$1x10^{-3}$	$1x10^{-2}$	$1x10^{-3}$	$1x10^{-3}$

Compression experiments were intended to be isothermal although a relatively small increase in temperature of up to 10°C occurred during some experiments. After compression, samples were quenched in water within 30s. Larger samples of 85mmØ x 150mm were hot isostatically pressed at 100MPa at 400°C for 4 h and then forged to a true strain of ~1 at strain rates $\sim 10^{-2}s^{-1}$ and $\sim 10^{-3}s^{-1}$ using a two step constant crosshead method. The microstructures at the centre of all samples were analysed by electron backscattered diffraction (EBSD) and energy dispersive spectroscopy (EDS), in a JEOL 6500 field emission gun SEM using TSL pattern acquisition and analysis software. In the EBSD orientation maps presented subsequently, high angle grain boundaries (>15°) are black and low angle boundaries are white. Elemental distributions were further analysed using electron probe microanalysis (EPMA) in a JEOL JXA8800 Superprobe equipped with four wavelength dispersive spectrometers.

3. Results and Discussion

3.1 Spraycast material

Figure 1(a) is an EBSD orientation map of the as-spraycast material showing an average grain size of ~10µm, an equiaxed grain morphology and a low fraction of as-sprayed porosity. Figure 1(a) indicated that, as intended, there were no large second phases or particles in the as-sprayed condition. Figure 1(b) is the Zr concentration distribution of the same material obtained using EMPA indicating some Zr-rich particles with adjacent regions relatively denuded of Zr. These particles were probably the coarse form of β'-Al_3Zr that formed in the mushy zone during solidification [5]. Further Fe and Si EPMA elemental maps are given elsewhere [4].

3.2 Hot consolidated material

The microstructure of the consolidated material is shown in the EBSD orientation map in Figure 2, where the grain boundaries were significantly more serrated than in the as-spraycast condition. Some grain boundary regions overcame the pinning effect of the dispersoid particles which led to an increase in the average grain size to ~11µm. Growth probably initiated in dispersoid-free-zones adjacent to the grain boundaries. Figure 2(b) shows the corresponding Zr distribution obtained using EDS compositional mapping, with grain boundaries superimposed. Coarse Zr-rich particles were located predominately at the grain boundaries (examples are arrowed), consistent with formation during the final stages of solidification. In other grain boundary regions, the Zr concentration was reduced and there were no Zr-rich particles.

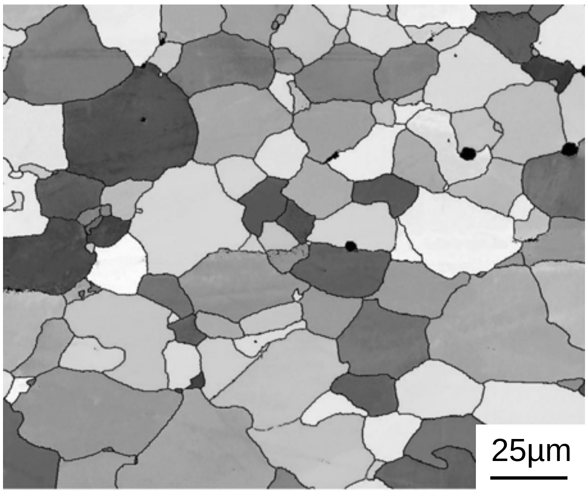

Figure 1(a): EBSD map of the Al-Mg-Li-Zr alloy in the as-spraycast condition, showing a fine equiaxed microstructure.

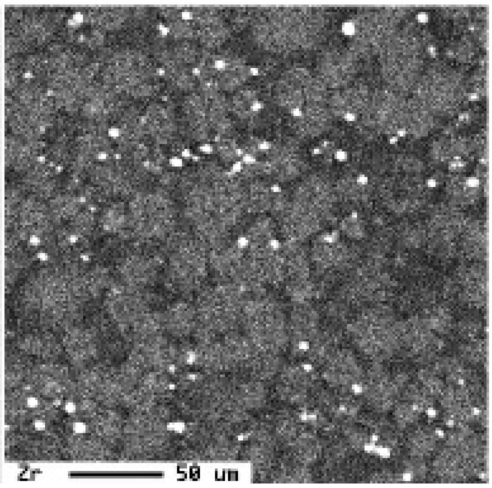

Figure 1(b): Corresponding EPMA Zr map, illustrating Zr rich particles and Zr denuded regions.

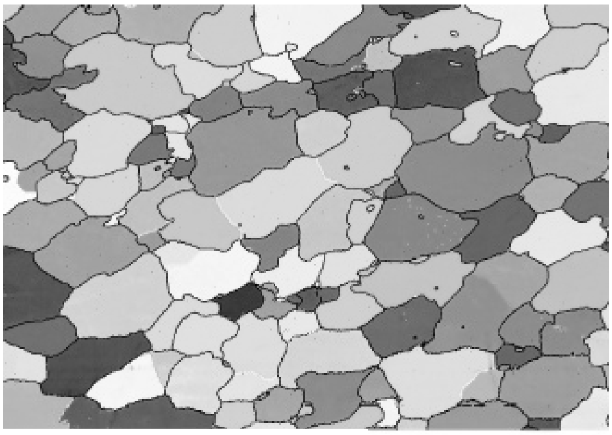

33.30 µm = 100 steps (a)

Figure 2(a): EBSD map of the hot consolidated alloy, showing a broadly equiaxed microstructure, but with more serrated grain boundaries.

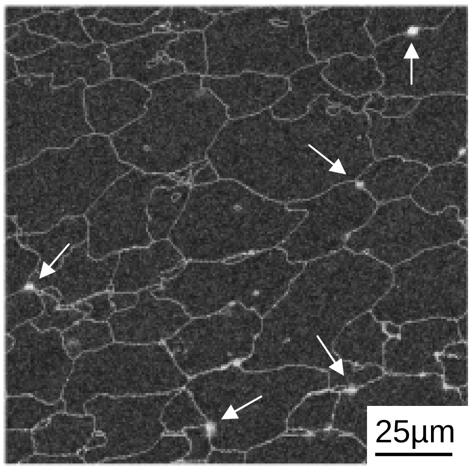

(b)

Figure 2(b): EDS Zr map with superimposed grain boundary map, illustrating Zr rich particles predominately at grain boundaries.

3.3 Hot compressed material

Typical EBSD orientation maps for hot compressed samples, in this case deformed at $10^{-3}s^{-1}$ to a true strain of 1 at 400, 325 and 250°C are shown in Figure 3 (a)-(c). The compression axis is horizontal.

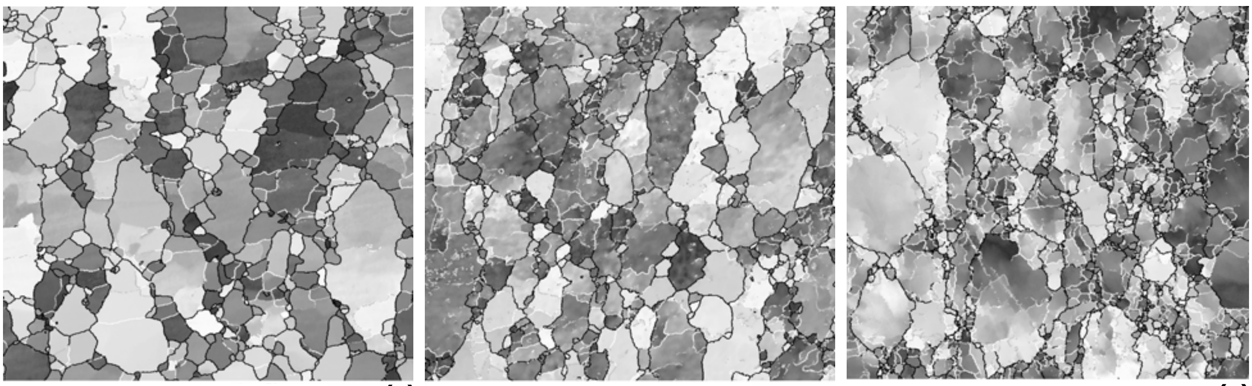

25.00 µm = 100 steps (a) 25.00 µm = 100 steps (b) 25.00 µm = 100 steps (c)

Figure 3: EBSD maps of samples (a) 400-1-2, (b) 325-1-2 and (c) 250-1-2. The average grain size decreased with decreasing deformation temperature.

Table 3 summarises the measured grain size and proportion of high angle grain boundaries (HAGBs) in the small grains, defined as grains with less than 500 data points, giving a typical threshold diameter of ~6µm, and assumed to be grains or sub-grains newly formed during compression. The measured average grain size was in the range 1.7-4.3µm, and decreased with decreasing deformation temperature and increasing total strain and strain rate. As the deformation temperature decreased, the area fraction of small grains A_f increased, spanning the range 0.14-0.36, and the proportion of HAGBs within the small grain population decreased, spanning the range 0.34-0.79.

Table 3: The effect of hot deformation conditions on key microstructural parameters.

	400-1-2	400-1-3	400-1.7-2	400-1.7-3	325-1-3	250-1-2	250-1-3	250-1.7-3
Average grain size (µm)	3.6	4.3	3.4	4.2	3.4	1.7	2.3	1.9
Small grain size (µm)	2.4	2.4	2.5	2.6	2.1	1.3	1.7	1.5
Large grain size (µm)	10.5	10.4	9.4	10.3	10.9	14.5	11.7	11.5
A_f small grains	0.19	0.14	0.32	0.19	0.16	0.18	0.24	0.36
Fraction HAGB in small grains	0.64	0.76	0.69	0.79	0.55	0.34	0.51	0.43
Zener-Holloman Factor (s^{-1})	2.38×10^{14}	2.38×10^{13}	2.02×10^{14}	2.02×10^{13}	1.89×10^{15}	1.18×10^{19}	4.76×10^{17}	1.01×10^{18}

Figure 4 is an EBSD orientation map from sample 250-1-2, partitioned into small and large grains according to the previous definition, showing the typical location of new small grains predominately at points of localised strain concentration and reduced fine dispersoid concentration associated with grain boundaries and triple points. It is speculated that the regions where large clusters of new grains were formed were regions of large difference in Schmid factor between adjacent grains, leading to increased local strain. Sample 250-1-2 showed that only 6% of HAGBs remained in the large grains, suggesting that virtually all of the grain boundaries and triple points had nucleated new grains.

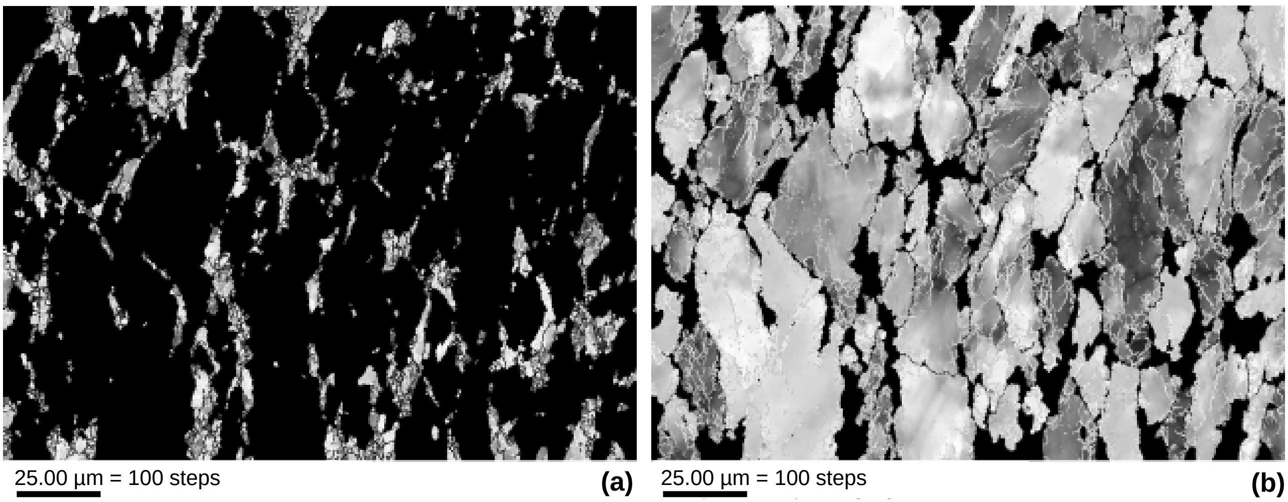

Figure 4: EBSD maps of sample 250-1-2, showing (a) small grains nucleated at grain boundaries and triple points, and (b) the large grains, with the majority of the prior grain boundaries and triple points annihilated by the formation of new small grains.

The proportion of HAGBs in the small grains decreased with decreasing temperature and increasing strain rate suggesting a shift from dynamic recrystallisation (DRX) to dynamic recovery (DRC). Menon and Rack [6] studied the effect of deformation conditions on binary Al-Li alloys and found qualitatively similar behaviour. However in the present work, the DRX regime is shifted to comparatively lower temperatures or higher strain rates. The lower temperature of this regime is attributed to the smaller initial grain size and the presence of dispersoids in this study.

The true stress versus true strain behaviour for all the samples during hot compression is shown in Figure 5(a) and can be consolidated using the Zener-Holloman parameter Z:

$$Z = \dot{\varepsilon}\exp(Q/RT) \quad (1)$$

where $\dot{\varepsilon}$, Q, R, and T are strain rate, activation energy, molar gas constant and absolute temperature respectively. Equation (1) is often recast as [7]:

$$\dot{\varepsilon} = A(\mathrm{SINH}\alpha\sigma)^n\exp(-Q/RT) \quad (2)$$

where A, α (the stress multiplier) and n are constants and σ is the stress taken from Figure 5(a). Using $\alpha = 0.052\mathrm{MPa}^{-1}$ [8] and best fitting the data to Equation 2 gave n~2 at 400°C and n~1 at 250°C, supporting a change in microstructural evolution mechanism over this range. The best fit activation energy $Q=215\mathrm{kJmol}^{-1}$ using n = 2 over the whole temperature range agreed well with $Q=205\text{-}219\mathrm{kJmol}^{-1}$ for other Zr dispersoid containing Al-Li alloys [9]. The activation energy was higher than $\sim150\mathrm{kJmol}^{-1}$ for self diffusion in Al [10] or Mg diffusion in Al [9], because of the presence of β'-Al_3Zr dispersoids.

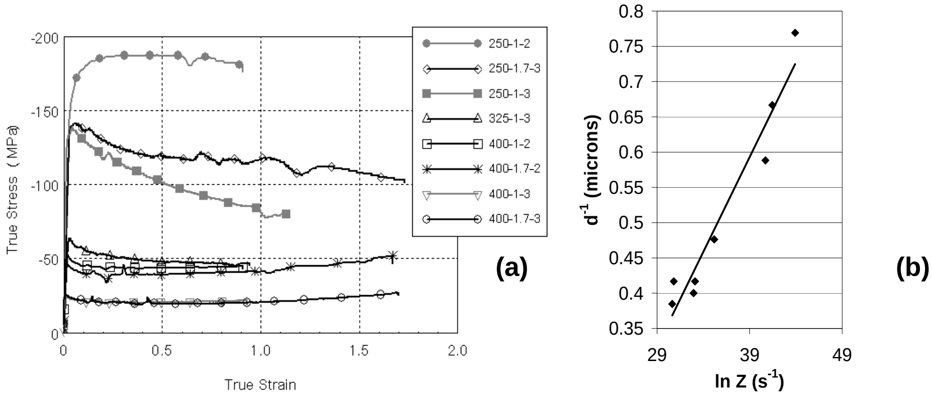

Figure 5: (a) True stress versus true strain data for during hot compression; (b) reciprocal of the small grain diameter (d^{-1} (μm^{-1})) versus ln Zener-Holloman Z factor for the data in (a).

The Zener-Holloman factor Z for each sample is given in Table 3. Figure 5(b) shows an approximately linear relationship between the small grain size d obtained from the EBSD data and the Z factor of the form:

$$d^{-1} = 0.027\ln Z - 0.45 \quad (3)$$

where the best fit regression coefficient R^2 = 0.94. Scatter in Figure 5(b) arose from variations in the deformation conditions during an experiment, e.g. difficulties in maintaining isothermal conditions, strain softening effects and likely differences in microstructural evolution with different temperatures. Nonetheless, these results are qualitatively consistent with those for 8090 and 8091 Al-Li alloys [9].

3.4 Large scale forging trials.

Figures 6(a) and (b) show EBSD orientation maps of HIPped and forged material with average grain sizes of 3.2µm and 4.5µm at strain rates of $10^{-2}s^{-1}$ and $10^{-3}s^{-1}$ respectively.

Referring to Table 3, the large scale forging grain sizes are similar to those for similar conditions in the small scale compression experiments, confirming that small scale testing was a valid and time-saving method to establishing suitable processing conditions for large-scale forgings.

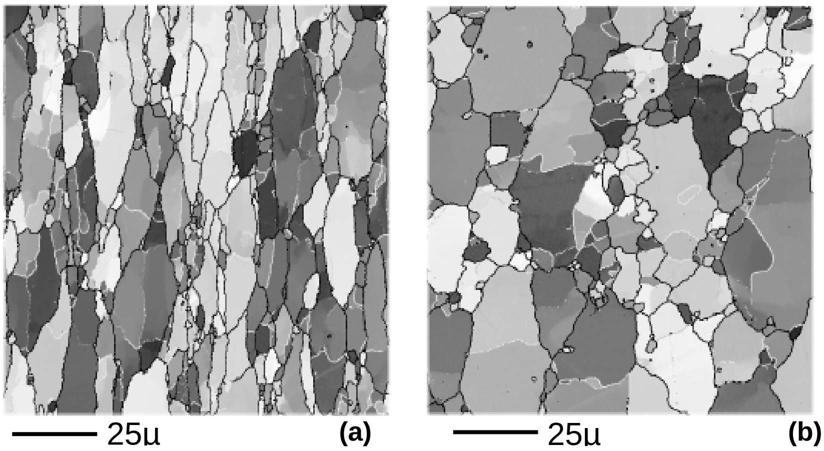

Figure 6: EBSD maps of HIPped, and forged material at a strain rate of (a) $10^{-2}s^{-1}$, and (b) $10^{-3}s^{-1}$.

4. Conclusions

1. As-spraycast Al-5.31Mg-1.15Li-0.28Zr had an initial grain size of ~10µm. After heat-treatment at 400°C for 4h the grain size coarsened only marginally. The Zr distribution was non-uniform, with denuded regions adjacent to coarse Zr rich particles at grain boundaries.
2. A range of grain sizes between 1.7 and 4.3µm arose during hot compression by either dynamic recrystallisation or dynamic recovery depending on conditions, predominately at grain boundaries and triple points. Overall, a smaller average grain size resulted from an increase in the Zener-Holloman factor Z and an increase in total strain. The fraction of high angle grain boundaries in the new grains decreased with decreasing grain size, indicating a shift from dynamic recrystallisation to dynamic recovery as Z increased.
3. Analysis of true stress versus true strain data showed the small grain size d was related to the deformation conditions by the relationship $d^{-1} = 0.027\ln Z - 0.45$.

4. Large scale forgings showed microstructures consistent with those in small scale compression experiments under similar conditions of temperature, strain and strain rate.

Acknowledgements

The authors would like to thank the UK Engineering and Physical Sciences Research Council, MoD and QinetiQ for financial support; QinetiQ for the large scale forgings; and C.J. Salter for help with EPMA.

References

[1] I.N. Fridlyander, A.G. Bratukhin and V.G. Davydov, Proc. Al-Li VI, DGM, 35, 1992.
[2] A. Charewicz and J.H. Weber, Proc. Al-Li VI, DGM, 569, 1992.
[3] P.S. Grant, Prog. Mater. Sci. 39, 497-545, 1995.
[4] I.G. Palmer, S.C. Hogg and P.S. Grant, in the present proceedings.

[5] EPSRC Final Report GR/J36853, Structure-Property Relationships in Spray Formed Al-Li Alloys.
[6] S.S. Menon and H.J. Rack, Mater. Sci. Tech. 17, 790-794, 2001.
[7] C.M. Sellars and W.J. McG. Tegart, Mem. Sci. Rev. Metall. 63, 731, 1966.
[8] G. Avramovic-Cingara, D.D. Perovic and H.J. McQueen, Met. and Mat. Trans. A. 27A, 3478-3490, 1996.
[9] H.J. McQueen and R.D. Ryan, Mater. Sci. Eng. A322, 43-63, 2002.
[10] R.W. Evans and G.R. Dunstan, J. Inst. Met. 99, 4-14, 1971.